Control of crystal polymorph in microfluidics using molluscan 28 kDa Ca^{2+}-binding protein†

Bozhi Ji,[a] Maggie Cusack,*[a] Andy Freer,[b] Phil S. Dobson,[c] Nikolaj Gadegaard[c] and Huabing Yin*[c]

Received 15th February 2010, Accepted 23rd July 2010
DOI: 10.1039/c0ib00007h

Biominerals produced by biological systems in physiologically relevant environments possess extraordinary properties that are often difficult to replicate under laboratory conditions. Understanding the mechanism that underlies the process of biomineralisation can lead to novel strategies in the development of advanced materials. Using microfluidics, we have demonstrated for the first time, that an extrapallial (EP) 28 kDa protein, located in the extrapallial compartment between mantle and shell of *Mytilus edulis*, can influence, at both micro- and nanoscopic levels, the morphology, structure and polymorph that is laid down in the shell ultrastructure. Crucially, this influence is predominantly dependent on the existence of an EP protein concentration gradient and its consecutive interaction with Ca^{2+} ions. Novel lemon-shaped hollow vaterite structures with a clearly defined nanogranular assembly occur only where particular EP protein and Ca^{2+} gradients co-exist. Computational fluid dynamics enabled the progress of the reaction to be mapped and the influence of concentration gradients across the device to be calculated. Importantly, these findings could not have been observed using conventional bulk mixing methods. Our findings not only provide direct experimental evidence of the potential influence of EP proteins in crystal formation, but also offer a new biomimetic strategy to develop functional biomaterials for applications such as encapsulation and drug delivery.

1. Introduction

Biomineralisation is the process of mineral synthesis by living organisms.[1–3] Molluscan biominerals, in particular, have attracted much attention due to the production of different polymorphs of calcium carbonate within a single shell.[1,2,4,5] The shell architecture of *Mytilus edulis*, for example, consists of an outer calcite layer and inner aragonite layer.[6,7] The contiguous formation of these two polymorphs is under exquisite biological control enlisting specific proteins and carbohydrates to form a robust shell.[8–10]

In bivalve molluscs the extrapallial (EP) fluid occupies a cavity between the mantle tissue and the shell and contains high concentrations of proteins, many of which have Ca^{2+}-binding properties and possibly dual functionality in the context of shell formation and heavy metal detoxification.[11] The model suggested by Addadi *et al.*[8] proposes that the mantle cells are in direct contact with the mineral.[8,12,13] The constant protein composition of the extrapallial fluid and the calcium-binding activity of the most abundant EP protein[11] supports the role of the extrapallial fluid as the source from which proteins are recruited to the site of biomineralisation.[12,14–16] Indeed, in red abalone, flat pearls were formed on inorganic substrates, such as glass or mica, inserted into the extrapallial space.[12,17]

[a] *Department of Geographical & Earth Sciences, University of Glasgow, G12 8QQ, UK. E-mail: hy@elec.gla.ac.uk, Maggie.Cusack@ges.gla.ac.uk*
[b] *Glasgow Biomedical Research Centre, 120 University Avenue, Glasgow, G12 8QQ, UK*
[c] *Department of Electronics and Electrical Engineering, University of Glasgow, G12 8QQ, UK*

† Electronic supplementary information (ESI) available: Method: construction of supersaturation ratio profiles on-chip. Video 1: time lapse recording of the crystal formation from the 50 mM $CaCl_2$ and 50 mM Na_2CO_3 in MOPS in the absence of proteins. See DOI: 10.1039/c0ib00007h

Insights, innovation, integration

Unraveling the role of individual proteins in the process of biomineralisation is challenging due to the complicated and dynamically variable nature of the biological system. Using microfluidics, we have created a highly controlled *in vitro* system that may well resemble aspects of the processes occurring in natural shell formation. This approach, where a range of diffusion gradients can be followed, provides scenarios akin to *in vivo* systems where the extrapallial fluid (EP) is supersaturated with respect to the shell mineral proteins. Using this novel approach, we demonstrate the critical role of the 28 kDa EP protein concentration gradient in crystal morphology and polymorph selection. In conventional bulk experiments this information is not accessible.

These observations highlight the necessity to fully characterise the plethora of EP proteins and to understand the role and function of individual proteins in the biomineralisation process. In this study we used EP fluid extracted from the common blue mussel, *M. edulis*.

The most abundant EP protein of *M. edulis* is a highly glycosylated dimer with a monomeric molecular weight of 28 kDa.[11,18] The protein is acidic (pI between 4.08 and 4.67) and has binding capacity for positive ions including Ca^{2+}, Mg^{2+}, Cu^{2+} and Mn^{2+}.[11,18] Although these characteristics suggest a possible role for this protein in biomineral shell formation, there is, so far, no direct experimental evidence that demonstrates its role in inorganic crystallogenesis.

To realise the aspiration of assigning functionality to these EP proteins requires a novel approach where experimental control at high temporal and spatial resolution is paramount and only small quantities of proteins are required. Recently we have demonstrated the potential of microfluidics as a new platform for understanding biomineralisation.[19] Many advantages of microfluidics over bulk systems have been demonstrated such as fast analysis, small sample consumption and excellent reproducibility.[20,21] These advantages have been exploited in life sciences *e.g.* cell engineering,[22] drug delivery[23,24] and protein studies.[25,26] Real time growth of $CaCO_3$ crystals in the presence of EP extracts was monitored on-chip with *in situ* Raman microspectroscopy to determine the resultant crystal polymorph.[19]

Here we look specifically at the calcium-binding activity of the most abundant EP protein. We demonstrate the power of microfluidics to probe the complex factors that control biomineralisation, providing insight into the influence of this specific protein that cannot be obtained from experimental crystal growth in bulk solutions.

2. Materials and methods

2.1 Materials and preparation

Reagents for calcium carbonate crystallisation: Calcium chloride ($CaCl_2$) and sodium carbonate (Na_2CO_3) were purchased from Sigma Aldrich. Extrapallial (EP) fluid proteins were extracted by syringe from the space between the mussel shell and the mantle tissue and then purified using ion exchange and gel filtration chromatography. Bovine serum albumin (BSA) and vitamin-D induced calcium binding protein (Sigma Aldrich) were used in protein experiments. All solutions were buffered in 100 mM MOPS buffer at pH 7.5.

2.2 Microfluidic device fabrication

T-junction microfluidic chips (Fig. 1) were made by casting polydimethylsiloxane (PDMS) elastomer against an SU-8 master as described elsewhere.[19] The total length of the serpentine microchannel was 5 cm, with all microchannels having a uniform cross section of 130 μm (width) × 100 μm (height). The PDMS was clamped against a cleaned glass substrate, forming a reversible seal, and microfluidic interconnects were created using established methods.[19] Reagents were delivered through the two inlets using syringe pumps (KD Scientific).

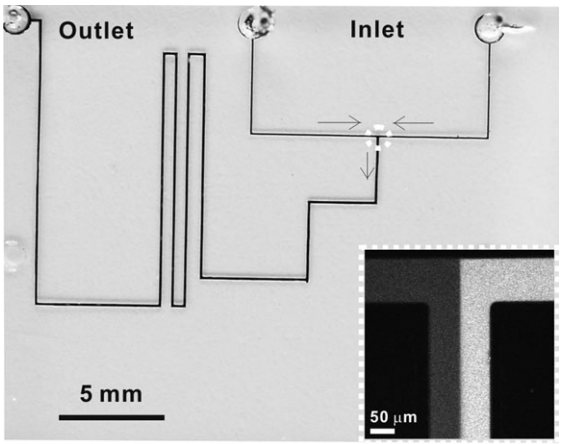

Fig. 1 Photography of the chip with a black dye solution in the channel. The inset shows a fluorescence image of the microchannel at the T-junction. A 1 μM fluorescein aqueous solution (bright) and deionised water (dark) were delivered from the two inlets to illustrate the formation of an interface.

2.3 Experimental settings for on-chip crystallisation

Microfluidics was used to identify the role of the 28 kDa extrapallial (EP) protein in the biomineralisation process by screening $CaCO_3$ crystal growth against a background of (i) 28 kDa EP protein, (ii) bovine serum albumin (BSA) (as a negative control since it has no Ca^{2+}-binding properties) and (iii) a 20 kDa calcium binding protein (Sigma) as positive control. Protein was added to the $CaCl_2$, Na_2CO_3 or both solutions as shown in Table 1 prior to on-chip experiments. Two concentrations of proteins were chosen, namely, 50 μg/ml and 10 μg/ml.

A small amount (5 μl) of the $CaCl_2$ and Na_2CO_3 solutions (described above) were delivered using carrier liquids at the same flow rate of 2 μl/min (*i.e.* 5.12 mm/s in the channel) through the two inputs respectively. Optical microscopy was used to record crystal formation and the resultant crystal morphogenesis. Duplicate on-chip experiments were carried out for *in situ* Raman monitoring of the crystal polymorph. Immediately after the experiments, the clamped chip was immersed in pure ethanol to separate the PDMS chip and the glass substrate. The PDMS chip was then dried with nitrogen for subsequent SEM imaging. No changes in crystal morphology and polymorph have been found to result from this treatment (at the optical resolution limit).

2.4 Bulk system for calcium carbonate crystallization

In order to compare the microfluidic system with traditional bulk calcium carbonate crystallization, each set of experiments

Table 1 Protein in reagents for crystallisation

Experimental Set	Inlet 1 50 mM $CaCl_2$	Inlet 2 50 mM Na_2CO_3
1	+	—
2	—	+
3	+	+
4	—	—

+: Protein was present in the solution. −: No protein was present in the solution.

was also carried out in bulk. Briefly, 100 μl each of the two solutions as described in section 2.3 was rapidly mixed for 1 min and then filtered through a 0.2 μm Millipore membrane, followed by rinsing with pure ethanol to preserve the crystals that formed. These crystals where then removed from the filter for Raman and SEM analysis.

2.5 Raman spectroscopy in polymorph identification

Raman spectroscopy was used for calcium carbonate crystal polymorph identification. Spectra were obtained from a LabRam INV Raman spectrometer (Jobin Yvon Ltd.) using a 632.81 nm laser beam as the excitation light source. Each spectrum was recorded with 10s integration time. An average of three spectral measurements on each crystal was used in the analysis. Both calcite and vaterite have a strong Raman peak at 1086 cm^{-1}. In vaterite, the corresponding peak is broader with a shoulder at 1074 cm^{-1}. Additional peaks at 710 and 281 cm^{-1} confirm calcite.[19]

2.6 Scanning electron microscopy

Scanning electron microscopy (SEM) was used to study calcium carbonate crystal morphology. The samples were sputter coated with gold/palladium and examined using a Hitachi SEM S-4700 with an acceleration voltage of 10 kV.

3. Results

3.1 Designing complex concentration profiles on-chip

Understanding the diffusion-controlled influence of proteins and ions in mineral formation is fundamentally important for informing our understanding of biomineralisation. Microfluidics provides an ideal platform for investigating such processes.

A typical microfluidic channel has dimension of tens of microns. At this scale, mass transport is diffusion controlled under laminar flow conditions. Thus, stable concentration gradients can be readily achieved in microfluidic devices. For the T-junction device used in this study, a flow velocity of 5.12 mm/s was applied to provide both laminar flow conditions and a range of concentration gradients along the length of the channel, so that a full range of crystal forming conditions could be assessed simultaneously.[19]

Fluidic computation is a powerful method that reveals mass transport in a complex system. Using computational fluid dynamics software (Comsol) we have previously constructed a complete set of concentration profiles for $CO_3^{2-}$and Ca^{2+} in a non-buffered system, the pH gradient and the distribution of supersaturation on-chip, monitoring the control of crystallisation by both pH and supersaturation.[19] To eliminate the influence of the pH gradient, MOPS buffer (100 mM) was used to keep Na_2CO_3 and $CaCl_2$ at pH 7.5—a physiologically relevant pH for this protein. Using the same calculations and taking into account the various carbonate, MOPS and pH equilibria, the supersaturation ratio (S) of this system was constructed (supplementary information) and is shown in Fig. 2A & Table 2. Although the overall shape of the supersaturation distribution is similar to a non-buffered system,[19] the value of S in this system is significantly lower. The supersaturation ratio of the system with 50 mM Na_2CO_3 and 50 mM $CaCl_2$ in MOPS has an S value of 7.4 which is almost an order of magnitude lower than the non-buffered equivalent while 10 mM Na_2CO_3 and 10 mM $CaCl_2$ in MOPS has an S value of 3.4 (Table 2).

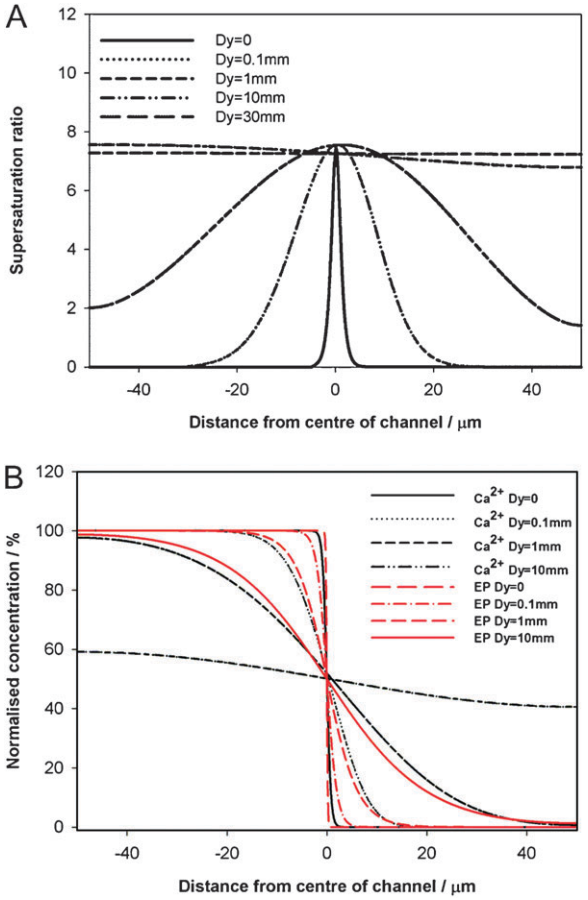

Fig. 2 Microfluidic simulation using the Nernst-Planck model with Comsol software. (A) profiles for supersaturation of Ca^{2+} and CO_3^{2-} ions across the channel at different distances in the direction of flow (Dy). The various acid–base equilibria and the MOPS buffer at pH 7.5 were taken into account in the simulation. The supersaturation ratio was calculated as previously.[19] (B) Normalized concentration profiles of Ca^{2+} and 28 kDa EP protein.

Table 2 Experimental maximum supersaturation ratios

System	Supersaturation ratio
10 mM Na_2CO_3 in DI water, pH 11.0 10 mM $CaCl_2$ in DI water, pH 4.9	53
10 mM Na_2CO_3 in 100 mM MOPS buffer, pH 7.5 10 mM $CaCl_2$ in 100 mM MOPS buffer, pH 7.5	3.4
50 mM Na_2CO_3 in 100 mM MOPS buffer, pH 7.5 50 mM $CaCl_2$ in 100 mM MOPS buffer, pH 7.5	7.4

Note: The formation of bicarbonate and carbonate is determined by the pH in the system. Based on the equilibrium among H_2CO_3, HCO_3, CO_3, bicarbonate is dominant in the system consisting of 50 mM Na_2CO_3 and 50 mM $CaCl_2$ in 100 mM MOPS buffer at pH 7.5. The concentration of bicarbonate (from calculations) is 46.9 mM in comparison to 0.07 mM of carbonate accounting for the much lower supersaturation ratios of $CaCO_3$ in the 100 mM MOPS buffer system.

The supersaturation ratio (S) is effectively a measure of the driving force of crystallisation such that systems with high S values tend to precipitate readily. Immediately after the delivery of $CaCl_2$ and Na_2CO_3 solutions into the chip, an interface formed at the start of the T-junction, where the maximum supersaturation ratio occurs. For the 50 mM $CaCl_2$ and 50 mM Na_2CO_3 in MOPS, rapid precipitation of crystals occurs as indicated by the formation of microscale crystals within 1 min (supplementary video 1). In contrast, no crystal formation occurs for the 10 mM $CaCl_2$ and 10 mM Na_2CO_3 in MOPS during the course of on-chip experiments. To enable fast on-chip screening of EP protein function, only the 50 mM $CaCl_2$ and 50 mM Na_2CO_3 in MOPS was used in the study.

The concentration of ions and proteins at any time and their location along and across the channel can be calculated by considering both flow rate (y-axis) and lateral diffusion (x-axis). These data can be used to determine the local environment of any species. The diffusion coefficient of a large protein molecule is significantly lower than for Ca^{2+} ions. As a consequence, a sharp protein concentration gradient persist over a greater distance (Dy = 10 mm) by which time the Ca^{2+} concentration has diffused to become largely uniform across the channel (Fig. 2B).

3.2 Screening the role of EP protein on-chip

Influence of 28 kDa EP protein. In the absence of any protein additives, rhombohedral calcite crystals with smooth surfaces were the dominant product, a similar phenomenon to that observed in the previous study.[19] In order to identify the influence of the 28 kDa EP protein during $CaCO_3$ crystal formation two protein concentrations of 50 and 10 μg/ml were used. The proteins were added to the buffered solutions of 50 mM $CaCl_2$ and/or 50 mM Na_2CO_3 in MOPS.

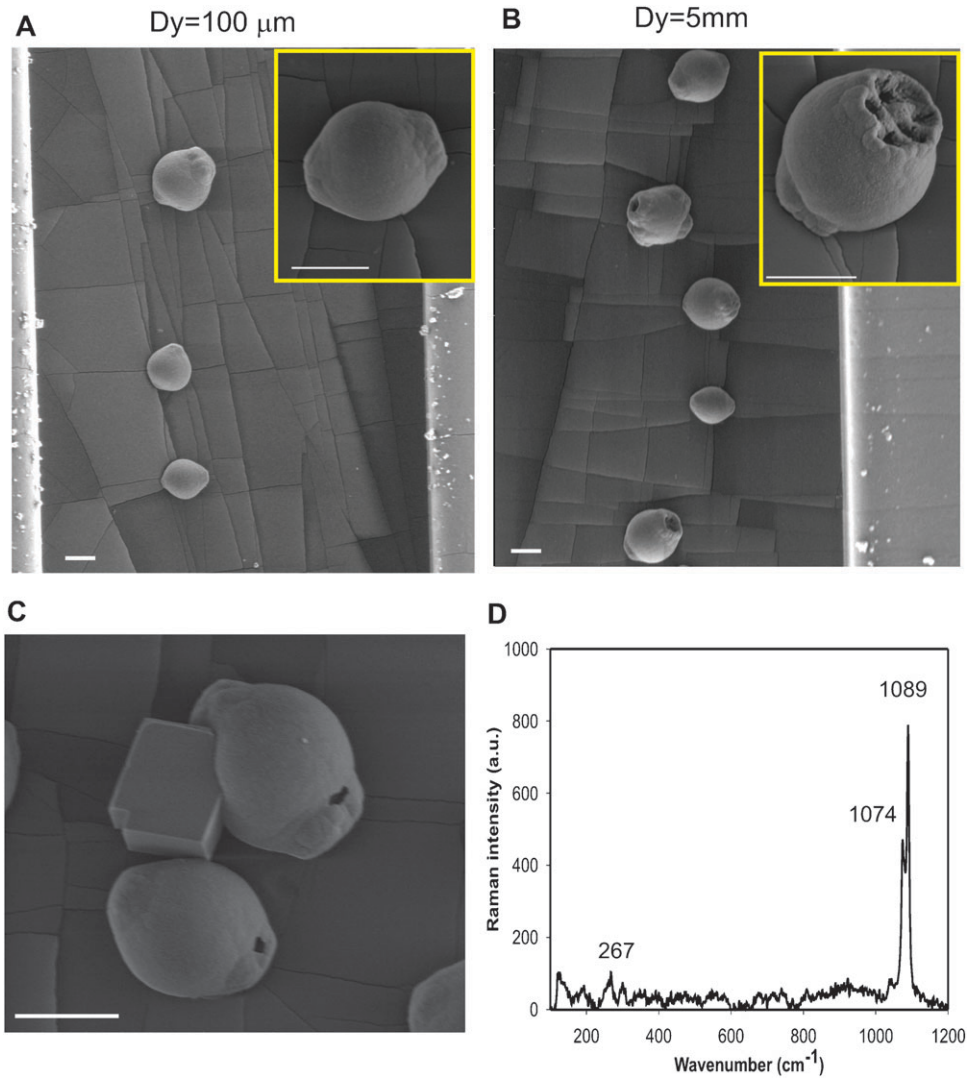

Fig. 3 Crystal formation in microfluidic channels with 50 μg/ml EP protein present in $CaCl_2$ solution only. SEM images of the crystals formed at the distances of (A) Dy = 100 μm and (B) Dy = 5 mm. High resolution images are given in the inserts. The lemon-shaped crystal in A is closed whereas the one in B is open. (C) At Dy > 5 mm, a calcite crystal grown out of lemon-shaped crystal. (D) Raman spectrum of the lemon-shaped vaterite crystal. All scale bars equal 10 μm. The cracked layers visible in the background of (A) and (B) are defects in the PDMS chip caused by gold coating prior to SEM imaging.

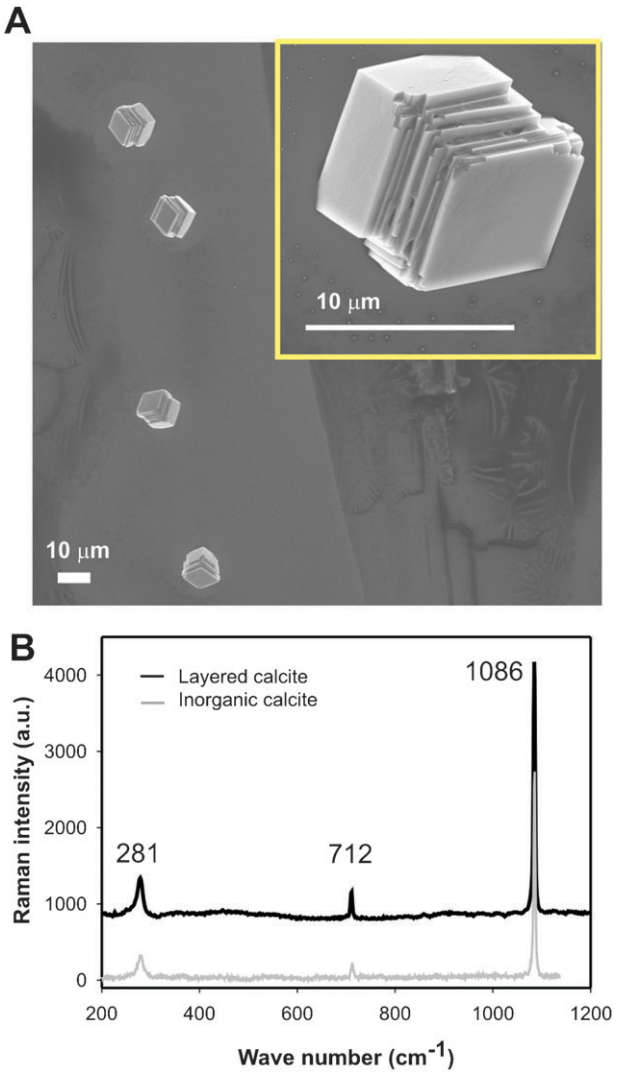

Fig. 4 A representative SEM image of crystals formed inside microfluidic channel when 50 μg/ml of EP protein was present in Na_2CO_3 solution only or in both Na_2CO_3 and $CaCl_2$ solutions. (A) Layered crystals were the only product formed, which were in the middle of the channel. Insert is a typical high magnification image of one of the crystals. (B) Raman spectrum of the layered crystal shows that it is the same as standard rhombohedral calcite formed in pure inorganic solutions (inorganic calcite).

Critically, the influence of the 28 kDa EP protein on crystal formation is dependent on which solution acts as the protein carrier. 28 kDa EP protein was added either to the $CaCl_2$ or Na_2CO_3 solutions, or both, prior to injection into the chip. Addition of 50 μg/ml of EP protein to the $CaCl_2$ channel produced predominantly hollow, lemon-shaped crystals near the starting point of the T-junction (Dy $<$ 100 μm) (Fig. 3A). These lemon-shaped crystals were uniform in size and closed (Fig. 3A, insert). The formation of similar crystals was observed along the channel (downstream at values of Dy $<$ 4 mm, data not shown). At the positions where Dy $>$ 5 mm, the dominant lemon-shaped crystals formed were open at both ends indicating a hollow structure (Fig. 3B, insert). In addition, calcite crystals started to form with many of them growing out of the lemon-shaped vaterite crystals, indicating a polymorph transition (Fig. 3C). Raman spectroscopy of the lemon shaped crystals (Fig. 3D) showed them to be the vaterite polymorph.

When 50 μg/ml of EP protein was added to either the Na_2CO_3 channel only, or to both channels, only the calcite polymorph was formed (Fig. 4A and B). However, these calcite crystals showed a distinct layered morphology, in contrast to the more familiar rhombohedral calcite obtained in the absence of any protein additive (denoted as inorganic calcite). The calcite layers were stacked parallel to each other although the edges were not perfectly aligned (Fig. 4A, insert). This stacking may indicate that a further role for the 28 kDa protein which may be in line with the classical crystallisation pathway of layer-by-layer growth due to adsorption of organic additives.[27,28]

Similar phenomena were observed at the lower concentration of 10 μg/ml for 28 kDa EP protein. The presence of 10 μg/ml EP protein in the $CaCl_2$ solution resulted in both layered calcite and hollow vaterite crystals (Fig. 5A). In this instance, most of the hollow crystals did not have the pronounced lemon-shape but had thinner shells. Many of the hollow crystals close to the initial meeting point of the two solutions (Dy $\sim$ 0), had open shells. High magnification SEM images reveal that these hollow crystals had a rough, granular surface comprising nano-particles of $\sim$40 nm (Fig. 5B). Further down the channel, as the diffusion processes reached equilibrium, only layered calcite was formed.

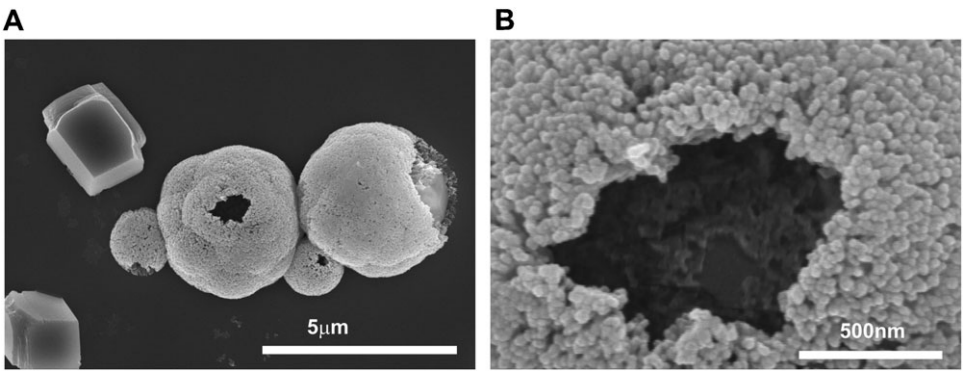

Fig. 5 Vaterite nano-granules at low EP protein concentration. (A) SEM images of crystals formed in microfluidics channel when 10 μg/ml of EP protein was in $CaCl_2$ solution only. Both hollow vaterite and calcite crystals were formed. Raman spectra for these are analogous to those shown in Fig. 3D and 4B respectively. (B) High resolution SEM image of a hollow vaterite structure shows its nano-granular composition.

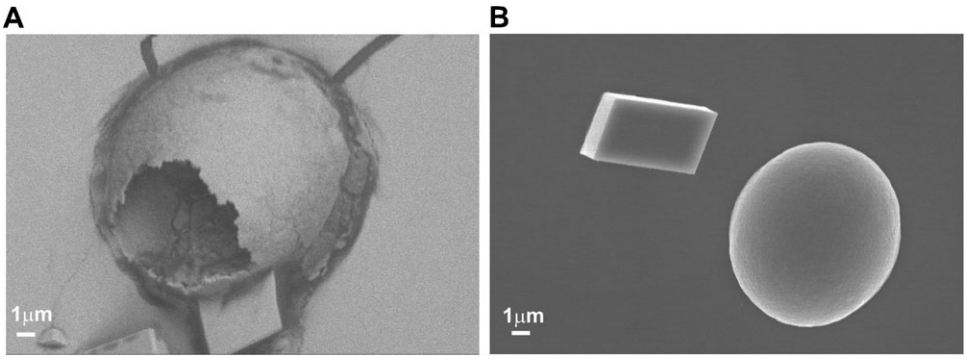

Fig. 6 Crystal formation inside microfluidics under positive control (calcium binding protein) and negative control (BSA protein). (A) The presence of calcium binding protein in $CaCl_2$ solution only gave rise to both open, thin shell vaterite and rhombohedral (and layered) calcite. Only calcite was formed when the calcium binding protein was present in Na_2CO_3 solution only or in both Na_2CO_3 and $CaCl_2$ solutions. (B) Both spheroidal vaterite and rhombohedral calcite was formed no matter which solution(s) delivered the BSA.

Positive and negative controls. The observed phenomena clearly show that the 28 kDa EP proteins affects $CaCO_3$ formation and suggests that it could influence biomineralisation of the molluscan shell. Although current knowledge is still far from identifying the functional groups of the EP protein and identifying how they might act in biomineralisation, its binding capacity for Ca^{2+} and Mg^{2+} provides a clue.[29] In order to confirm that it is the calcium-binding activity that is key in this role, 50 μg/ml of commercially available calcium binding protein (CaBP) was used for on-chip crystallisation under the same conditions as the 28 kDa EP protein. Similar results were found. When the CaBP was added to the $CaCl_2$ solution only, both calcite and hollow vaterite crystals were formed (Fig. 6A), whereas, as before, only calcite formed for the other conditions.

Bovine serum albumin (BSA) has no calcium-binding activity. It is unlikely to be involved in biomineralisation and therefore serves as a non-functional protein control. BSA was added to $CaCl_2$ only, Na_2CO_3 only, or both solutions. In all three cases, both solid, spherical vaterite and rhombohedral calcite crystals formed (Fig. 6B).

3.3 Screening the role of EP protein in the bulk system

Recently, there is increasing evidence that Ca^{2+} binding acidic polymers, including poly-aspartic acid (PolyAsp) and poly-acrylic acid (PAA), induce the formation of hollow spherical vaterite crystals *via* a polymer induced liquid precursor (PILP) process where amorphous calcium carbonate (ACC) nano-particles (*ca.* 20–30 nm) act as a template for growth.[30] Further work by Han *et al.* demonstrated that AAC spheres, at very low concentrations of PAA, surface crystallized to give hollow vaterite spheres.[31] Since all of these experiments were performed in a bulk system,[31–33] a bulk approach was employed in order to compare bulk and microfluidic systems for the influence of the 28 kDa EP protein. The EP protein was dissolved in $CaCl_2$, Na_2CO_3 or both solutions before the two solutions were mixed. In all of these combinations, only single rhombohedral calcite and calcite aggregates formed with no evidence of hollow vaterite crystals (Fig. 7). It is worth noting that the rapid mixing in a bulk system is driven by a turbulent flow and thus no stable concentration gradients are formed.

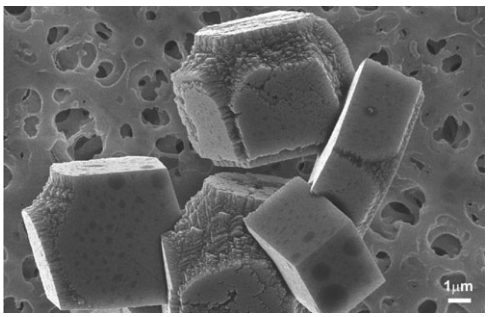

Fig. 7 SEM image of some crystals formed in a bulk system. Only single rhombohedral and aggregated calcite crystals formed with no evidence of vaterite crystals.

4. Discussion: findings in context of biomineralisation

Understanding the mechanisms of *in vivo* biomineralisation and the possible function of the 28 kDa EP protein has been investigated using microfluidics. This approach, where a range of diffusion gradients can be followed, provides scenarios akin to *in vivo* systems where no single set of experimental parameters occurs. As protein diffuses across ionic concentration gradients, different crystal polymorphs form. For the first time, we demonstrate the critical role of the 28 kDa EP protein concentration gradient in crystal morphology and polymorph selection with the formation of lemon-shaped, hollow vaterite crystals occurring only where stable EP protein and Ca^{2+} gradients co-exist.

This highly controlled *in vitro* system may well reflect the processes that occur in nature and enable a new approach to explore these. The rich EP protein concentration within the EP fluid, which is in contact with the growing shell surface, is in marked contrast to the low concentration of the insoluble shell matrix proteins.[29] Supersaturation and ionic diffusion gradients may provide the mechanism by which the protein influences mineral formation. One possible scenario is that the 28 kDa EP protein forms an active EP-Ca^{2+} complex in the initial stages of biomineralisation within the extrapallial cavity that is mobilised by diffusion driven transport. Diffusion controlled growth of calcite on surfaces has previously been demonstrated.[34]

High resolution SEM images reveal that the lemon-shaped crystals consist of aggregates of ~40 nm nanoparticles, although it is difficult to identity the nature of the individual nanoparticles, Raman spectroscopy showed the crystals were vaterite. These nanoparticles may indicate that the crystals could be formed by the recently described crystallisation mechanism of nanoscopic prenucleation clusters aggregating to form amorphous nanoparticles that develop crystalline domains.[35–37] It has also been demonstrated that the resultant crystalline polymorph (*e.g.* vaterite, calcite) is dependant on specific conditions, especially when additives are present.[14,35] In line with these studies, we have also observed the slight difference in the morphology of the lemon-shaped vaterite formed with 50 μg/ml and 10 μg/ml EP proteins as well as 50 μg/ml CaBP (Fig. 3, 5 and 6). Calcium binding capacity and protein concentration play a significant role in the processes associated with nanoparticle stabilisation and assembly. Further studies are required to reveal the precise mechanism.

In contrast to the bulk system used in most studies, the microfluidic approach allows us to define the location and profile of the supersaturation on-chip in real time, where *in situ* crystal formation occurs. In addition, the interplay between supersaturation and protein transport profiles can be realised on the same device. For example, in the lemon-shaped crystal formation, near the starting point of the T-junction, both sharply constrained supersaturation and EP protein concentration profiles present limiting conditions, leading to the uniform formation of the lemon-shaped crystals (Fig. 3). In contrast, further along the channel (Dy = 10 mm), the low supersaturation is distributed uniformly across the channel in the X-direction. However, at this point there is still a moderately steep EP protein concentration gradient, resulting in a much broader scope for interplay of the different solution components, generating variation in the size, morphology (opening of the lemon-shaped crystals) and polymorph. In theory, if the channel was long enough to make a uniform distribution in terms of supersaturation and EP protein concentration profiles, the majority of crystals formed at this point would be layered calcite, similar to the result seen when the 28 kDa EP protein was present in both solutions. Hollow vaterite spheres do occur in bulk systems in the presence in poly-acrylic acid (PAA),[31,38] presumably as a consequence of the stronger polyelectrolyte activity of PAA compared to the 28 kDa EP protein.

5. Conclusions

Using microfluidics we have demonstrated for the first time, that EP proteins located in the EP fluid adjacent to the shell, can regulate, at both micro- and nanoscopic levels, morphology, structure and polymorph. Most importantly, this regulatory influence is predominantly dependent on the existence of an EP protein concentration gradient and its interaction with Ca^{2+} ions. Novel lemon-shaped hollow vaterite structures with a clearly defined nanogranular assembly are formed when the 28 kDa EP protein is present only in the Ca^{2+} solution and there is a protein concentration gradient. In the absence of either of these two conditions, the presence of the 28 kDa EP protein results in layered calcite. Notably, discovery of these findings would not be possible using conventional bulk mixing methods.

Diffusion associated processes may be critical in the kinetic control of biomineralisation. Such processes can be systematically created and screened on a single chip at high spatial and temporal resolution. Subsequently, a large amount of rigorously correlated information is obtained on the same chip, which may shed light on the possible mechanisms underlying biominersalisation, such as non-classical crystallisation involving nanoparticle aggregation and self-assembly.[28] Our findings not only provide direct experimental evidence of the influence of the 28 kDa EP protein in crystal formation, but also offers a new biomimetic strategy to develop functional biomaterials for applications such as encapsulation and drug delivery.

Acknowledgements

H.Y. is supported by Royal Society of Edinburgh (RSE) as a RSE Personal Research Fellow. B.J. holds a Lord Kelvin/Adam Smith scholarship from the University of Glasgow. A.F. and M.C. gratefully acknowledge support from BBSRC (Grant BB/E025110/1). P.S.D is supported with an RCUK Academic Research Fellowship. We thank Professor Jon Cooper and Dr Andrew Glidle for constructive discussions throughout the project. Khedidja Mosbahi is thanked for initial protein purification.

References

1 M. Cusack and A. Freer, *Chem. Rev.*, 2008, **108**, 4433–4454.
2 M. Cusack, D. Parkinson, A. Freer, A. Perez-Huerta, A. E. Fallick and G. B. Curry, *Mineral. Mag.*, 2008, **72**, 569–577.
3 S. Weiner, *J. Struct. Biol.*, 2008, **163**, 229–234.
4 F. Nudelman, B. A. Gotliv, L. Addadi and S. Weiner, *J. Struct. Biol.*, 2006, **153**, 176–187.
5 N. P. Gong, J. L. Shangguan, X. J. Liu, Z. G. Yan, Z. J. Ma, L. P. Xie and R. Q. Zhang, *J. Struct. Biol.*, 2008, **164**, 33–40.
6 J. England, M. Cusack, P. Dalbeck and A. Perez-Huerta, *Cryst. Growth Des.*, 2007, **7**, 307–310.
7 W. T. Hou and Q. L. Feng, *Cryst. Growth Des.*, 2006, **6**, 1086–1090.
8 L. Addadi, D. Joester, F. Nudelman and S. Weiner, *Chem.–Eur. J.*, 2006, **12**, 980–987.
9 M. H. Schmidt, I. Ellison, K. Holliday, M. Kubin and F. Trujillo, *J. Cryst. Growth*, 2008, **310**, 804–815.
10 G. Falini, S. Albeck, S. Weiner and L. Addadi, *Science*, 1996, **271**, 67–69.
11 Y. Yin, J. Huang, M. L. Paine, V. N. reinhold and N. D. Chasteen, *Biochemistry*, 2005, **44**, 10720–10731.
12 A. M. Belcher, P. K. Hansma, G. D. Stucky and D. E. Morse, *Acta Mater.*, 1998, **46**, 733–736.
13 L. Addadi and S. Weiner, *Angew. Chem., Int. Ed. Engl.*, 1992, **31**, 153–169.
14 D. Gebauer, H. Colfen, A. Verch and M. Antonietti, *Adv. Mater.*, 2009, **21**, 435–441.
15 M. Truchet, M. Delhaye and C. Beny, *Analysis*, 1995, **23**, 516–518.
16 M. F. Butler, W. J. Frith, C. Rawlins, A. C. Weaver and M. Heppenstall-Butler, *Cryst. Growth Des.*, 2009, **9**, 534–545.
17 M. Fritz, A. M. Belcher, M. Radmacher, D. A. Walters, P. K. Hansma, G. D. Stucky, D. E. Morse and S. Mann, *Nature*, 1994, **371**, 49–51.
18 S. J. Hattan, T. M. Laue and N. D. Chasteen, *J. Biol. Chem.*, 2001, **276**, 4461–4468.
19 H. B. Yin, B. Z. Ji, P. S. Dobson, K. Mosbahi, A. Glidle, N. Gadegaard, A. Freer, J. M. Cooper and M. Cusack, *Anal. Chem.*, 2009, **81**, 473–478.

20 H. B. Yin, N. Pattrick, X. L. Zhang, N. Klauke, H. C. Cordingley, S. J. Haswell and J. M. Cooper, *Anal. Chem.*, 2008, **80**, 179–185.
21 C. E. Sims and N. L. Allbritton, *Lab Chip*, 2007, **7**, 423–440.
22 S. Y. Teh, R. Lin, L. H. Hung and A. P. Lee, *Lab Chip*, 2008, **8**, 198–220.
23 B. H. Weigl, R. L. Bardell and C. R. Cabrera, *Adv. Drug Delivery Rev.*, 2003, **55**, 349–377.
24 L. F. Kang, B. G. Chung, R. Langer and A. Khademhosseini, *Drug Discovery Today*, 2008, **13**, 1–13.
25 C. Sauter, K. Dhouib and B. Lorber, *Cryst. Growth Des.*, 2007, **7**, 2247–2250.
26 B. T. C. Lau, C. A. Baitz, X. P. Dong and C. L. Hansen, *J. Am. Chem. Soc.*, 2007, **129**, 454–455.
27 W. Kossel, *Ann. Phys.*, 1934, **413**, 457–480.
28 F. C. Meldrum and H. Colfen, *Chem. Rev.*, 2008, **108**, 4332–4432.
29 Y. Yin, J. Huang, M. L. Paine, V. N. Reinhold and N. D. Chasteen, *Biochemistry*, 2005, **44**, 10720–10731.
30 L. A. Gower and D. A. Tirrell, *J. Cryst. Growth*, 1998, **191**, 153–160.
31 J. T. Han, X. R. Xu and K. W. Cho, *J. Cryst. Growth*, 2007, **308**, 110–116.
32 J. G. Yu, J. C. Yu, L. Z. Zhang, X. C. Wang and L. Wu, *Chem. Commun.*, 2004, 2414–2415.
33 A. H. Cai, X. R. Xu, H. H. Pan, J. H. Tao, R. Liu, R. K. Tang and K. Cho, *J. Phys. Chem. C*, 2008, **112**, 11324–11330.
34 J. Aizenberg, A. J. Black and G. M. Whitesides, *Nature*, 1999, **398**, 495–498.
35 B. P. Pichon, P. H. H. Bomans, P. M. Frederik and N. A. J. M. Sommerdijk, *J. Am. Chem. Soc.*, 2008, **130**, 4034–4040.
36 D. Gebauer, A. Volkel and H. Colfen, *Science*, 2008, **322**, 1819–1822.
37 E. M. Pouget, P. H. H. Bomans, J. A. C. M. Goos, P. M. Frederik, G. de With and N. A. J. M. Sommerdijk, *Science*, 2009, **323**, 1455–1458.
38 N. Loges, K. Graf, L. Nasdala and W. Tremel, *Langmuir*, 2006, **22**, 3073–3080.